To appear in Brain Research, *vol. 1536, pp. 2-15.*
http://www.sciencedirect.com/science/article/pii/S0006899313010548

The speed of learning instructed stimulus-response association rules in human: Experimental data and Model.

Guido Bugmann[1], Jeremy Goslin[2], Patricia Duchamp-Viret[3]

[1]Centre for Robotics and Neural Systems. [2]School of Psychology.

University of Plymouth. Drake Circus. Plymouth PL4 8AA. United Kingdom.

[3]1UMR 5292, Centre de recherche en neurosciences de Lyon, Université de Lyon, CNRS, INSERM, 50 avenue Tony Garnier, F-69366 Lyon, France

gbugmann@plymouth.ac.uk, jeremy.goslin@plymouth.ac.uk, pviret@olfac.univ-lyon1.fr

Keywords: Rapid instructed task learning, Pre-frontal cortex, Inferior-temporal Cortex, Hippocampus, synaptic learning

Abstract

Humans can learn associations between visual stimuli and motor responses from just a single instruction. This is known to be a fast process, but how fast is it? To answer this question, we asked participants to learn a briefly presented (200ms) stimulus-response rule, which they then had to rapidly apply after a variable delay of between 50 and 1300ms. Participants showed a longer response time with increased variability for short delays. The error rate was low and did not vary with the delay, showing that participants were able to encode the rule correctly in less than 250ms. This time is close to the fastest synaptic learning speed deemed possible by diffusive influx of AMPA receptors. Learning continued at a slower pace in the delay period and was fully completed in average 900ms after rule presentation onset, when response latencies dropped to levels consistent with basic reaction times. A neural model was proposed that explains the reduction of response times and of their variability with the delay by i) a random synaptic learning process that generates weights of average values increasing with the learning time, followed by ii) random crossing of the firing threshold by a leaky integrate-and-fire neuron model, and iii) assuming that the behavioural response is initiated when all neurons in a pool of *m* neurons have fired their first spike after input onset. Values of *m*=2 or 3 were consistent with the experimental data. The proposed model is the simplest solution consistent with neurophysiological knowledge. Additional experiments are suggested to test the hypothesis underlying the model and also to explore forgetting effects for which there were indications for the longer delay conditions.

1. Introduction

A unique human skill is the ability to understand task instructions. For instance: “Each time there is an animal in the pictures I will show you, press the red button”. Over the years, numerous psychophysical experiments have made use of this ability. However, only recently has research started to focus on how the brain converts instructions into mental programs. This is the area of “instruction-based learning (IBL)” (Bugmann, 2009, Ruge and Wolfensteller, 2010; Bugmann, 2012, Hartstra et al., 2012, Wolfensteller and Ruge, 2012) or “rapid instructed task learning (RITL)” (Cole et al., 2010).

The observations that IBL i) takes at most a few seconds (see e.g. Ruge and Wolfensteller, 2010), ii) is a one-shot process and iii) is assumed to establish relations between distant brain areas, have triggered the development of a computational model of fast learning across several neuronal relays Bugmann (2009, 2012). However, there were no hard data on the actual speed of human learning and no clear information on how fast synapses can learn that could be used to constrain a model.

The questions addressed in this paper are: How fast is “fast” learning? Is the behavioural learning time consistent with the hypothesis that Stimulus-Response (SR) rules are encoded in synaptic weights?

To answer the first question (section 2), we set up an experiment to determine the actual behavioural learning time of humans. In this experiment, participants were visually presented for a very short time (200ms) with a stimulus-response rule to learn. After a time interval of between 50 and 1300ms they were then asked to apply the rule. The expectation was that they would not be able to reply before learning was completed, causing increased response times for short intervals.

Answering the second question was more convoluted. First, we established what anatomical pathways were most likely to support fast learning (section 3). Secondly, we used pathway assumptions to analyse the experimental response times in terms of a constant propagation time added to a delay-dependent rule retrieval process, allowing us to characterize the learning element of the circuit (section 4). We then sought to explain the characteristics of the learning element in terms of synaptic learning rule and firing of a leaky integrate-and-fire (LIF) model of a neuron, or a number of those (section 5). Once we were satisfied that a LIF model-based neural system could explain the data, we used that model to infer the values the synaptic weight values reached after different delays in the experiment. This revealed the time course of synaptic learning during SR rule presentation and in the delay before rule retrieval.

The results of this work show that experimental data are consistent with an involvement of the hippocampus in both simple reaction time tasks and SR encoding and retrieval tasks. These require synaptic modifications as fast as seems physically possible. The variability of the response times is consistent with a few independent neurons being required to encode the SR rule.

2. Experiment

2.1 Method

2.1.1 Participants

Eleven people, eight male and three female, participated in this experiment with ages ranging from 21 to 62 years (mean = 42.9 years, sd = 13.96 years).

2.1.2 Procedure

Participants were required to learn a simple stimulus-response (SR) rule and then rapidly apply that rule to a single following stimulus. The rule instruction took the form of an image showing a capital letter in the middle of the image along with either a left-pointing or right-pointing arrow, also placed to the left or the right of the letter (Fig. 1B). The letter indicated the stimulus and the arrow the required response, a key press performed using right or left index finger (left or right shift key on keyboard). This rule was displayed for 200ms, followed by a blank screen with a duration (termed the "delay" *D*) randomly selected from 50, 100, 300, 500, 700, 900, 1100, or 1300 ms. After the blank screen, the test stimulus was presented until the response was produced or until a 5 second timeout (Fig 1A). If the test stimulus was the same letter as that used in the previously displayed SR rule then participants had to react using either left or right index fingers according to the arrow indicated by the rule. If the stimulus did not correspond to letter of the prior rule then participants were asked to press the space bar with either thumb. Each session consisted of a list of 160 SR rules randomly created from combinations of each of 26 capital letters and left and right response directions. Of these, there were 96 trials where the stimulus matched that used in the rule, and 64 where there was a mismatch. Each session was preceded by 20 baseline reaction time measurements, where participants immediately responded to left or right arrows by pressing keys with left or right index fingers as quickly as possible. After this, five familiarisation trials of the main procedure were run. Participants completed such a session four times, each time with a different random ordering of the 160 trials. Each session took approximately 8 minutes to complete, with participants typically leaving a few hours between each session.

To appear in Brain Research, *vol. 1536, pp. 2-15.*
http://www.sciencedirect.com/science/article/pii/S0006899313010548

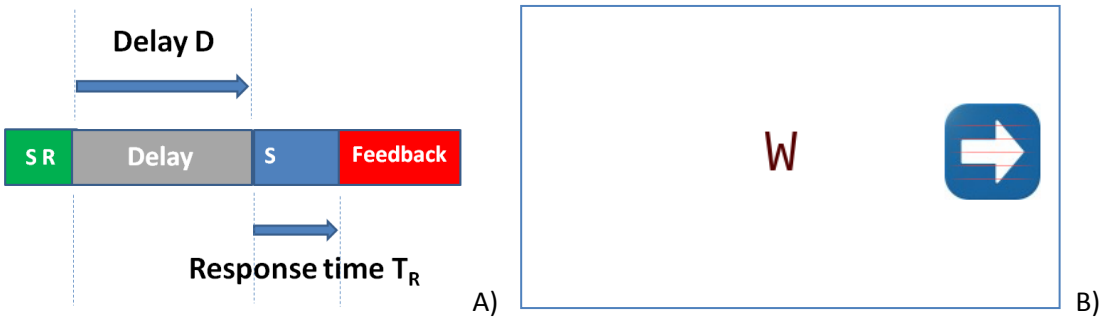

Figure 1. A. Time line of the experiment. The Stimulus-Response rule is presented for 200ms. The delay *D* varies between 50ms and 1300ms. B. Format of the Stimulus-Response (S-R) rule presentation. In this example, the arrow instructs to press the right shift key (Response R) when the stimulus W is presented alone

The experiment was designed using the free software OpenSesame (Mathôt et al., 2012), in Legacy mode, and run on Windows XP laptops. This mode is most stable but can add 15-20 ms to recorded response times (Mathôt et al., 2012). Participant response times (t_R) were measured from the onset of the stimulus. It was expected that response times for longer delays would be a constant for each participant, based upon the time required to recall the association and respond accordingly (Fig 2). However, with shorter delays it was expected that the stimulus would be presented before the learnt association could be established. In these cases there would be an increase in response time that would also include latencies that would reflect the additional time required to complete the formation of the SR association.

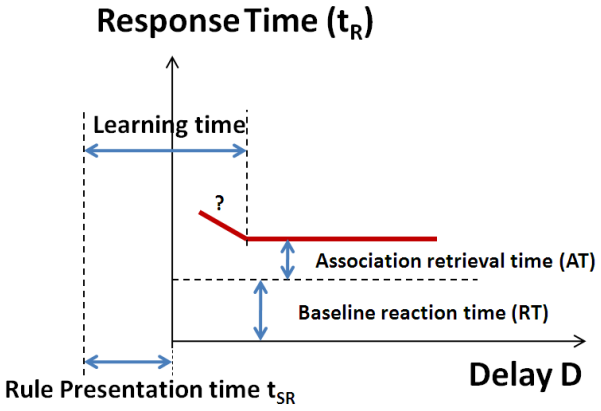

Figure 2. Conceptual response expectation. If the stimulus is presented before learning is completed, the measured response time (full thick line) is expected to deviate from a constant value defined by the association retrieval time AT and the baseline reaction time RT.

One of the reasons for using letters of the alphabet as stimuli is that participants had already developed connections to recognize these, allowing the experiment to focus on learning the associative part of the task.

2.2 Results

2.2.1 Accuracy

Overall participants had responded accurately to 94.02% of stimuli. An ANOVA analysis of the distribution of accurate responses over the four sessions and eight different delay times did not reveal any significant ($F < 1$) main effect or an interaction between these factors.

2.2.2 Reaction Times

The response times in each SR trial were measured from the onset of the stimulus, and were only considered for analysis if they originated from trials with correct responses. For each delay, there were 12 measurements with target part of the SR rule and 8 with a non-target.

Mean response times were calculated for each participant across each combination of the four sessions and for eight delay times. During these calculations, outlier removal was performed by rejecting responses of less than 100ms, greater than 2000ms, and those that fell outside of 2.5 standard deviations of the cell mean. The same procedure was also applied to the 20 baseline RT trials that preceded each session. These values were then subtracted from responses of the corresponding session of the SR Task, giving us latencies free from between-participant variance in baseline RT, and are summarised in Figure 3.

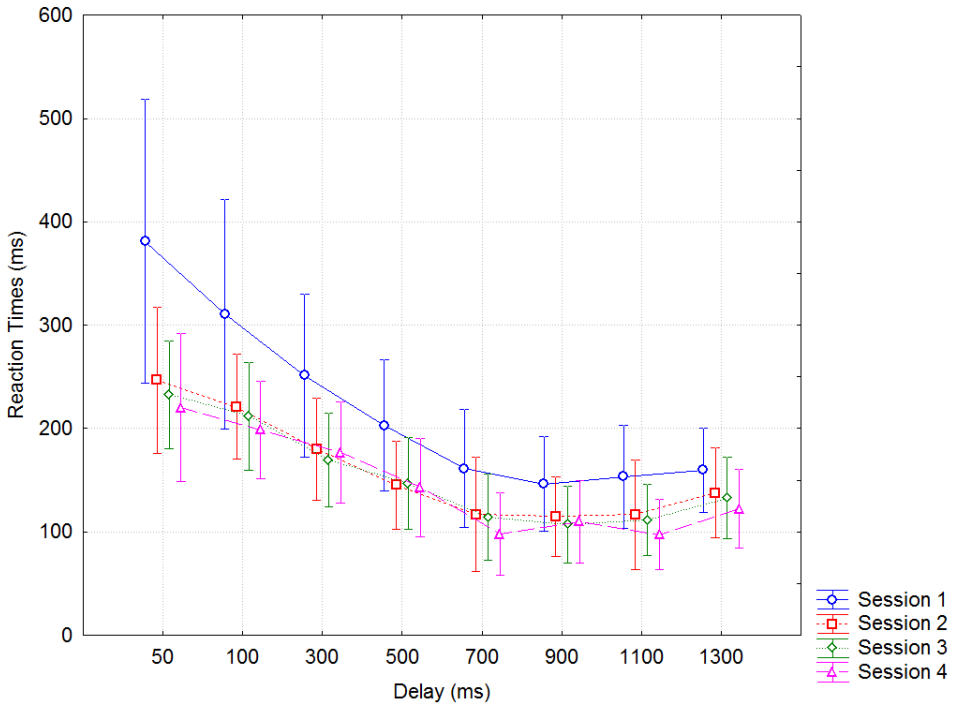

Figure 3. SR task reaction time latencies across the four sessions and eight delay conditions. Error bars represent 0.95 confidence intervals.

These data were then used as the dependant variable in a repeated measures ANOVA with within-participant factors of session (1-4) and delay (50, 100, 300, 500, 700, 900, 1100, 1300ms). In cases

where Mauchly's test revealed a violation of the assumption of sphericity reported significance values were corrected using Greenhouse-Geisser estimates. This analysis revealed a significant of delay ($F(7,42)=25.63$, $\eta^2= .72$, $p < 0.001$), a significant interaction between the session and delay ($F(21,210)=3.90$, $\eta^2= .28$, $p < 0.001$), and a marginal effect of session ($F(3,18)=3.86$, $\eta^2= .28$, $p = 0.059$).

A posthoc examination of latency differences between delay conditions, shown in Figure 4, was conducted using paired-sample t-tests between RTs for each of the conditions. These revealed that RTs for the 50ms delay were significantly ($p < 0.05$) greater than those of all the conditions with longer delay durations. This was also the case for the 100, 300, and 500ms delay conditions. RTs for the 700ms delay condition were not found to be significantly different from those of the 900 ($t = 0.42$), 1000 ($t = 0.44$), or 1300ms ($t =-1.89$) delay conditions. Neither was there a significant difference between RTs between the 900 and 1100ms delay conditions ($t = -0.02$). However, RTs for the 900ms condition were found to be significantly less than that of the 1300ms condition, with RTs for the 1100ms condition also significant less than that of the 1300ms condition. As we will attempt to replicate this pattern of using neural models we have made an attempt to verify their findings by making each of the paired-sample posthoc t-tests subject to Monte-Carlo simulation with 1000 different random permutations of participant-specific averages between the delay conditions. These simulations did not highlight any differences to the pattern of significance.

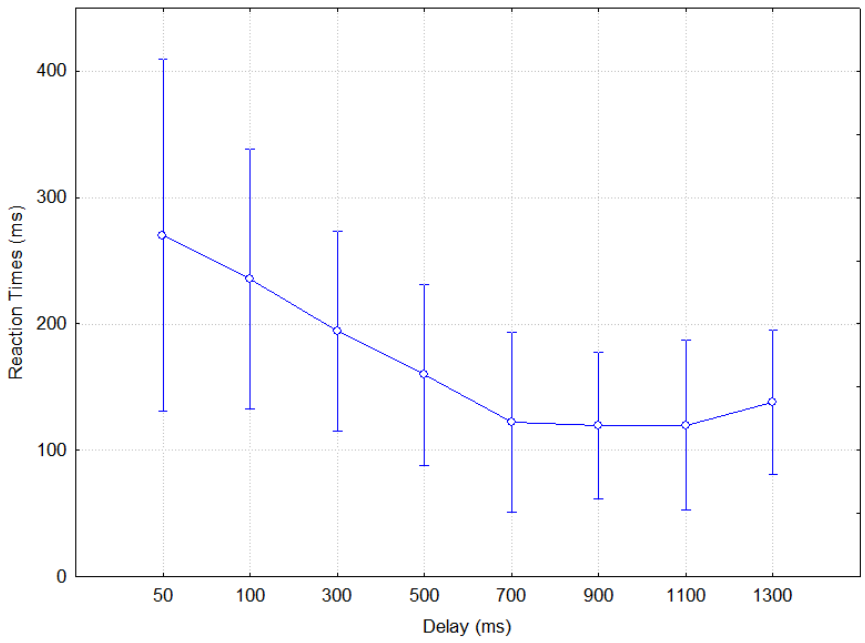

Figure 4. SR task reaction time latencies across eight delay conditions when collapsed across the four session conditions. Error bars represent 0.95 confidence intervals.

Examination of the interaction between the experiment factors of session and delay were made by conducting further ANOVAs testing for the effect of session in each of the delay conditions, and testing for the effect of delay in each of the sessions. The former of these series of analyses revealed that there was a significant effect of session in the 50 ($F(3,30)=6.68$, $\eta^2= .40$, $p < 0.05$) and 100ms ($F(3,30)=4.15$, $\eta^2= .29$, $p < 0.05$) delay conditions, but not in any of the longer delays (300ms: $F(3,30)=3.17$, $\eta^2= .24$, $p = 0.088$; 500ms: $F(3,30)=2.56$, $\eta^2= .07$ $p = 0.12$; 700ms: $F(3,30)=2.42$, $\eta^2= .08$,

p = 0.14; 900ms: F(3,30)=1.52, η^2= .13, p = 0.25; 1100ms: F(3,30)=2.78, η^2= .21, p = 0.094; 1300ms: F(3,30)=1.11, η^2= .1, p = 0.35). Posthoc pairwise t-tests of the effect of session in the 50 and 100ms delays revealed the same pattern of significance. That is, response times were significantly longer in session 1 than the other three sessions, with no significant difference between response times in sessions 2, 3 and 4. In the next series of analyses we examined whether there was an effect of delay in each of the four sessions, with ANOVAs revealing significant effects of delay in each session (Session 1: F(7,70)=17.75, η^2= .64 p < 0.001; Session 2: F(7,70)=19.25, η^2= .66, p < 0.001; Session 3: F(7,70)=20.5, η^2= .67, p < 0.001; Session 4: F(7,70)=13.15, η^2= .57, p < 0.001). Further posthoc testing of the effect of delay within each session revealed a very similar pattern of significance to that of the main effect of delay in the original analysis. Finally, we then performed separate ANOVA analyses of the interaction between session and delay on each different pairwise combination of the four sessions. These revealed significant interactions between session and delay when comparing session 1 with sessions 2 (F(7,70)=4.76, η^2= .32, p < 0.05), 3 (F(7,70)=5.88, η^2= .37, p < 0.01), or 4 (F(7,70)=6.03, η^2= .38, p < 0.01). However, there was no significant interaction (F < 1) in any of the pairwise comparisons between sessions 2, 3 and 4.

2.2.3 Response time variability

In order to examine the response generation process, we investigated the relation between the standard deviation of the response time with the average response time. Figure 3 indicates that the response process has reached a stable state in sessions 2, 3 and 4. Therefore we focus on these sessions. Fig 5 shows the relation between time to response from the moment the stimulus is shown and its standard deviation.

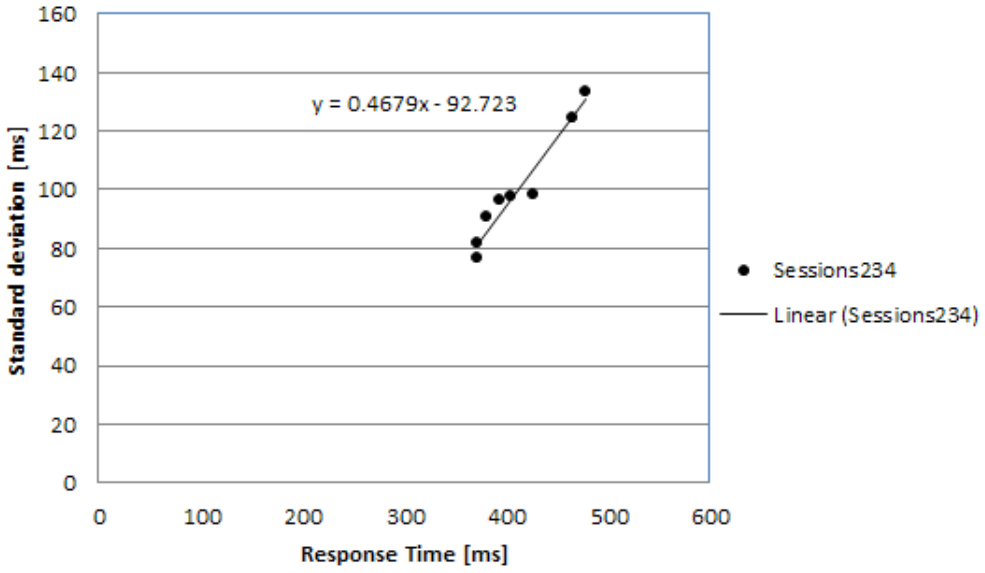

Figure 5. Standard deviation (SD) of the time to response *Tr* from the moment the test stimulus S that was part of the learnt SR rule is shown. The full circles symbols correspond to the average Tr and their SD for each value of the delay D, averaged over all subjects and sessions 2, 3 and 4. The linear fit represents the relation between SD and Tr for sessions 2, 3 and 4.

This relation is typical of two random processes operating in series, with a clear linear relationship between SD and reaction times combined with a consonant RT delay. This can be described as follows:

$$Tr = T_1 + T_2(D), \qquad (1)$$

where T_1 is a random process with a constant average $\overline{T}_1$ and variance SD_1^2, and T_2 has a variable average $\overline{T_2}(D)$ depending on the delay D, and a variance $SD_2^2(D)$ that increases with the average. One could, for instance, identify T_1 with the information propagation process and that of muscle activation, and assume T_2 to be the process of retrieval of the associated response from memory. The latter is then assumed to reflect the quality of SR encoding controlled by the value of D. If the parameters of T_1 can be estimated, then the properties of T_2 can be isolated. For this, we can make use of following relations that are valid if T_1 and T_2 are independent random processes.

$$SD^2(Tr) = SD^2(T_1) + SD^2(T_2(D)) \qquad (2)$$

$$\overline{Tr} = \overline{T}_1 + \overline{T_2}(D) \qquad (3)$$

To discover the properties of $T_2(D)$ we have four pieces of experimental information *Tr*, *SD(Tr)*, *RT*, *SD(RT)*[1]. Both include a propagation time component. Whether it is possible to extract properties of $T_2(D)$ depends on the anatomical pathways used by the two tasks, the simple reaction time task and the rule retrieval task. Possible anatomical pathways are discussed in section 3.

The average of the RT over sessions 2, 3 and 4 is 315ms with a standard deviation SD(RT)=87ms.

2.3 Summary of results

The main finding of this experiment is that participants experience a significant increase in response time when applying an SR rule if a stimulus is presented less than 700ms (200ms rule presentation + 500ms delay) after the presentation of the rule.

The error rate was small at all delays, with no significant effect of the delay, indicating that for a learning time of 250ms (200ms presentation time + 50ms delay), there was already a fully functional encoding of the rule. The improvements in performance for longer learning times can be taken as an indication for a further strengthening of the encoding with time.

Another effect observed in this experiment is the difference between the sessions, in that response times for delays equal to or less than 100ms were found to be significantly longer in the first session than any of the subsequent sessions. Session 1 appears to be a task acquisition session leading to a more stable response pattern for subsequent sessions.

The response times curves show three phases. First, for short delays, there is a significant decrease of the response times with increased delays. In phase two, the response times then flattens out,

[1] In the reminder of the paper, we will use the symbol Tr and RT for average values.

until phase three around D=1300 where a significant increase in response time is observed. This increase correlates with subjects reporting a difficulty in remembering the rule for long delays. This could indicate the start of the decay of the encoded memory. Following parts of this paper focus on modelling phase one and two.

The relation between response time and its standard deviation suggests that two random processes in series shape the behavioural response time.

3. Anatomical basis for S-R learning

Several pathways link visual input to finger movements as motor output. There is the traditional dorsal route, from V1 to V3, AIP, PMv (F5) and motor cortex (M1) (see e.g Sakata et al., 1997) with possibly two sub-routes (Grafton, 2010). AIP and F5 are the parietal and pre-motor regions respectively of hand and finger movement control. Recent data show that there are strong inputs to AIP from the ventral visual stream (area TE) (Borra et al., 2008). This enables a possible "ventral" route from V1 to V4, Tea/TEp, AIP, PMv, M1. A third route has been suggested by Passingham and Toni (2001) from V1 to TE, PFC (46v) and PMv.

A number of converging evidences point to the ventral route as a good candidate for fast S-R learning.
Several participants reported using "visual memory" to recover the action associated with the stimulus letter. The literature on associative visual memory shows that neurons in infero-temporal cortex (IT and its sub-areas TE, all representing the central visual field (Ungerleider et al., 2008)) were able to fire as if an absent visual pattern were present, upon presentation of its associated cue (see review in Osada et al., 2008). Experimental data by Naya et al., (1996) show that, when two stimuli have been associated during previous training, some IT neurons that normally respond to one of the two stimuli, also fire when the other stimulus is presented. According to Naya et al. (1996) this pair-recall effect is seen as part of mental imagery supported by information retrieval from long-term memory. Such associative memory retrieval required the perirhinal area 36 to activate area TE, with an additional input from PFC (Ranganath et al., 2004). Brasted et al. (2003) argued that the hippocampus was required for "fast" learning of stimulus-response associations, although the term "fast" referred to tens of presentations. The hippocampal area CA1 is bi-directionally connected to area 36 (Naber et al., 1999; Furtak et al., 2007, Kealy and Commins, 2011). CA1 could therefore act as the associative memory feeding back a representation of the response to area 36 upon presentation of the stimulus.
Recall-related activity has been observed in the human (Gelbard-Sagiv et al., 2008) and monkey Hippocampus (Rolls and Xiang, 2006). In the one-trial learning experiment by Rolls and Xiang (2006), the observed response errors indicated that the recall cells coded for the place to be touched, not the actual movement to be done. A similar disconnection between recall and response was observed in IT by Messinger et al. (2005). This is what would be expected from a visual memory of the instruction.

Regarding the response action initiation, several experiments have pointed to the lateral parietal area IPS (including AIP) as a necessary relay to produce the response in a learnt S-R rule (Bunge et al,

2002). This makes the direct link between TE and PFC a less likely route to action. However, this link is required for learning associations between visual stimuli and motor responses and between two visual patterns. It is also needed for the retrieval of learnt associations (Bussey et al., 2002). The ventro-lateral PFC (VLPFC) is identified in multiple experiments as a necessary component of a S-R learning system (see review in Bunge et al., 2002. The VLPFC is bidirectionally connected to area TE (Rempel-Clower and Barbas , 2000) and modulates activity in the inferior temporal cortex (Fuster et al., 1985), areas TE and 36 (Zironi et al., 2001). TE receives input from PFC lateral areas 12, 46v. Area 36 receives input from more orbital PFC areas 11, 12 (Rempel-Clower and Barbas , 2000). On the basis of lesion studies, Passingham et al. (2000) suggested that areas 12/45a are part of the circuitry that forms associations between visual cues and the actions they specify. The rostral part of PFC area 12 (12r) is connected to AIP, TE and PMv (Borra et al., 2011) and appears to be well placed to control the learning and execution of S-R rules.

The hippocampus does not receive direct inputs from PFC, but could be influenced via the VLPFC projections to area 36 and orbito-frontal to area 28 (entorhinal cortex) (Rempel-Clower and Barbas , 2000).

The association circuit is summarised in figure 6. In the model developed in this paper, we propose that the PFC interacts with the ventral visual stream, from TE to 36/28, to store and retrieve associations, while the link between TE and AIP conveys the selected response towards the motor cortex. PFC inputs to all these areas allow controlling learning and recall. These assumptions appear to be consistent with the available data on conditional visuo-motor associative learning and with anatomical data. The concept is consistent with results of Mruczek and Sheinberg (2007) showing that associative IT firing preceded action initiation and the strength of firing is correlated with the speed of the response. Thus, associative firing in IT appears to be a key step in task generation[2].

There is a lack of measurements on S-R learning as fast as reported here. Many results come from experiments with trial-and-error learning lasting at least several minutes, analyzed with methods admittedly lacking temporal resolution (e.g. Murray et al., 2000). Existing electrophysiological data are not informative on fast learning. For PFC, several reports (e.g. Asaad et al., 1998) describe neurons in area 46, possibly including area 12, that responded to the stimulus, the response, and the conjunction of both, during trial-and-error learning. Other PFC data focus on the retrieval of well learnt associations (e.g. Yamagata et al., 2012). Similarly, data from TE and 36 are collected under conditions of retrieval (Osada et al., 2008). One FMRI experiment in humans was conducted with visual rule instructions as in our experiment, and with data analysis focusing on the execution phase after learning (Ruge and Wolfensteller, 2010). The results inform on the changes of brain activity with repeated retrieval of four S-R rules, with IPS (including AIP) and PFC showing a decrease, while PM and visual areas showed an increase. These studies also showed a reduction in the response time by 60ms with practice. The hippocampus and IT showed no significant activation above baseline during retrieval. Our experiment also measures retrieval, but with very short retrieval delays, to probe early stages of the learning process.

[2] How perceptual information in IT/TE becomes mapped to action information in AIP does not appear to be documented. We assume that this has happened prior to associative learning, in the early stages of session 1.

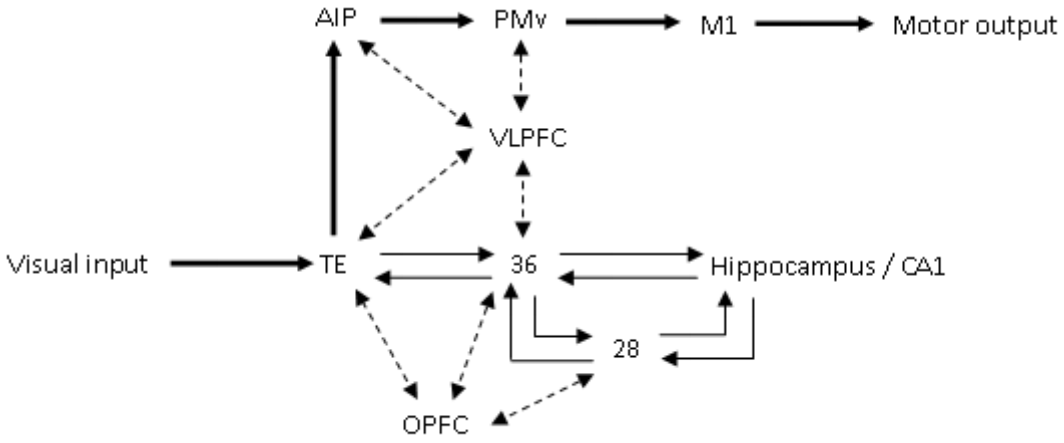

Figure 6. Summary of the circuit proposed to implement the S-R task. The S-R rule is stored in the Hippocampus and the retrieved image of the desired response is fed back to area TE where it is mapped to a motor action via AIP. VLPFC and OPFC are managing the encoding and retrieval process. The thick line indicates a possible faster route, based on associations encoded in TE.

In our model we will assume that during learning the fact that a letter and an arrow appear together is encoded in weights able to activate the representation of either member of the pair when presenting the other. The image of the arrow, actual or generated, is picked up in TE to produce a response via AIP. The mapping between the representation of the arrow in TE and the representation of the action in AIP is assumed to be learnt during reaction time measurements, prior to the S-R experiment. Similarly, we assume that TE has already built representations of letters.

It will be assumed that learning of the association between the representation of the stimulus and that of the response is Hebbian (Hopfield, 1982)and is supported by the visually-driven activation of both representations. At the end of the S-R presentation, activity and learning continues with the support of feedback from the PFC. During that time, the motor output is inhibited by the control circuit to prevent the activity representing the arrow from triggering an action.

When the test stimulus is presented, PFC is inhibited by the control circuit, the motor system is dis-inhibited, and the response is generated through the newly created connections.

4. Data interpretation

The literature points strongly at an involvement of the hippocampus in rule encoding and retrieval measured by Tr. However, when reacting to existing associations, such as in the simple baseline reaction time task, there are several possible routes. The shortest goes directly from TE to IP, as shown in Figure 7A. As can be seen this route would incur a propagation delay through the network of r_1 and r_2, plus r_0. The latter represents the minimal firing time of a neuron when its weights are set to maximal values, where the delay is essentially determined by the arrival rate of input spikes. Therefore the total delay using this route can simply be expressed as:

$$RT = r_1 + r_2 + r_0, \qquad \text{(A-4)}$$

An alternative route for simple reaction times (not involving learning) might also involve the hippocampus, as shown in Figure 7B. This would incur delays further to the previous route by the addition of propagation delays r3 and r4, an extra r_0, plus T_{20}, similar to r_0. T_{20} is the minimal delay of a fully trained T_2 process. Therefore, the total delay using a hippocampus base RT route would involve a delay of:

$$RT = r_1 + r_0 + r_3 + T_{20} + r_4 + r_0 + r_2 \qquad \text{(5)}$$

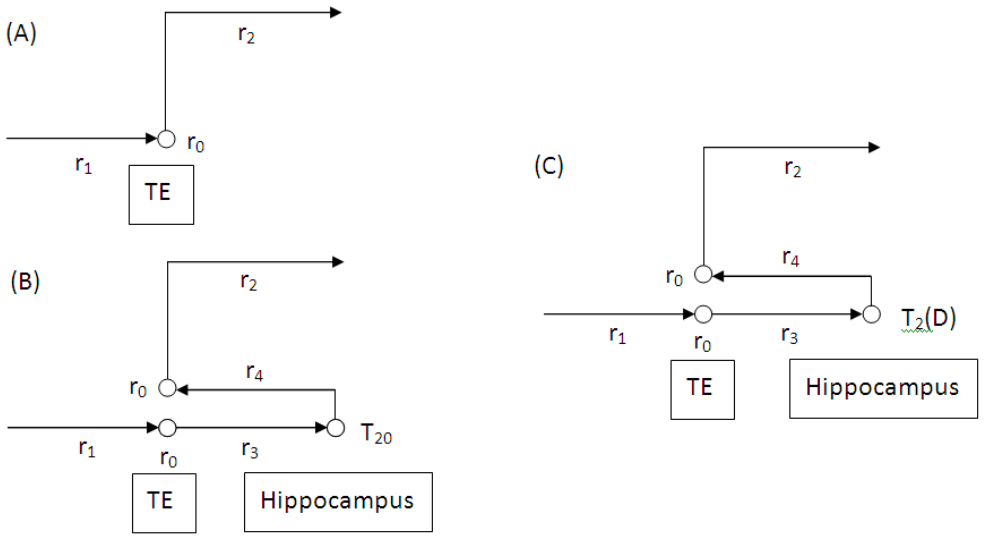

Figure 7. Considered anatomical paths for the simple RT task (A, B) and for the S-R retrieval task (C). Delays are explained in the text.

Our aim is to investigate and model the variability of TR, as measured by its standard deviation SD shown in Fig. 7C, focussing upon the learning-specific delay T2(D), and the response time of neurons with partially trained weights due to the training time limitation to T_{SR} + D.

If we assume the routes (A) and (B) for the base RT then, after learning, the Tr becomes either:

$$Tr_a = RT + r_0 + r_3 + r_4 + T_2(D). \qquad \text{(6)}$$

or

$$Tr_b = RT - T_{20} + T_2(D) \qquad (7)$$

Assuming that right-hand terms are independent processes, the variances SD^2 of the response time are given by:

$$SD_a{}^2(Tr) = SD^2(RT) + SD^2(r_0 + r_3 + r_4) + SD^2(T_2(D)) \qquad (8)$$

$$SD_b{}^2(Tr) = SD^2(RT) + SD^2(T_{20}) + SD^2(T_2(D)) \qquad (9)$$

If we plot $\sqrt{SD^2(Tr) - SD^2(RT)}$)) versus *Tr-RT* for both routes (figure 8A), assuming a known underlying relation between $SD(T_2(D)$ versus Tr-RT, we can see that, the $SD(T_2(D))$ versus *Tr-T* curve is shifted to the right for routes A and C and left for routes B and C. The amount of right-shift is the minimum response time r_0 of a TE neuron plus the propagation time r_3+r_4 between TE, the hippocampus and back. The amount of left shift is the minimal delay T_{20} of a fully trained process T_2.

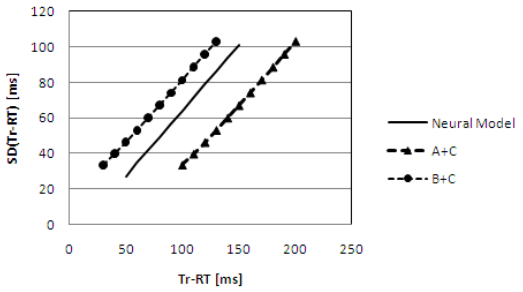

A)

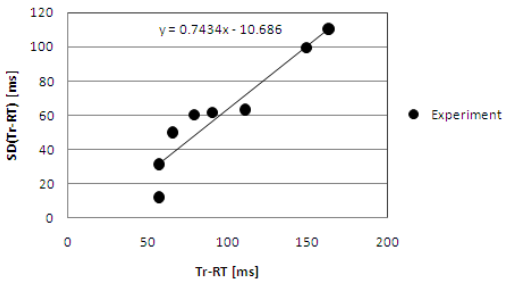

B)

Figure 8. A. Expected behaviour of a plot of $\sqrt{SD^2(Tr) - SD^2(RT)}$ versus *Tr-RT* calculated from experimental data for two different connectivity models A+C and B+C. The continuous line represents the behaviour of the underlying retrieval process. The flanking doted lines represent the result of the calculation applied to experimental data to produce figure B. **B.** Experimental behaviour of the SD calculated from data in figure 5. See the text for details of the calculations done.

Figure 8A shows that the calculation of the properties of *Tr-RT* essentially shifts the curve of the retrieval process T2(D) laterally, but does not change its slope significantly.

Figure 8B shows the curve calculated from data in figure 5 and the experimental reaction time data. The horizontal axis represents *Tr(D)-RT* (RT=315ms). The vertical axis represents $\sqrt{SD^2(Tr) - SD^2(RT)}$. For *SD(RT)* we had to use a lower value (76 ms) for the standard deviation of *RT* (SD(RT)=87 ms). This was required because the experimental standard deviation of *Tr* at D=900 ms was just above 76 ms.

To estimate the robustness of this result, we simulated the process in formula (1) using the parameters from RT in section 2.2.3 for process T_1 and generated 400[3] normally distributed random times for 8 different average times from 50 ms to 225 ms, with process T_2 with a standard deviation set by $SD_2 = 0.74*T_2$. The same analyses were done as for the experimental data and fitting the results by $y=ax+b$ as in figure 8B were conducted. After 25 new random sets, the average slope a was 0.743 (SD = 0.051) and the average intersection b was -0.66 (SD = 8.01). The averages were close to the expected values. The intersections showed a greater variability than the slopes. We concluded that our experimental slope value of 0.743 is close to the actual biological value of the average participant, that probably lies between 0.69 and 0.79. The experimental intersection is less reliable, but the biological one is probably negative, signalling a progressive increase of the slope of *SD(T)* for retrieval times smaller than those observed here.

To determine which route is more consistent with the data, we examined the behaviour of a model of the learning and retrieval process (section 5). The aim was to generate a curve for the underlying process similar to that in figure 8A, and to use it to determine whether the data were more consistent with the use of route (a) or (b).

5. Modelling learning and retrieval mechanisms.

The experimental relations between delay and response time, and between the standard deviation of the response time and the response time can be used to constrain a model of SR learning and retrieval.

Here, we explore a model hypothesis involving mechanisms and connections that are coarsely consistent with the physiology and anatomy of the brain. We consider that i) the SR rule is encoded as increased synaptic weights ii) Learning is assumed to start when the SR rule is presented, continues during the delay and ends when the test stimulus is presented. Learnt weights are used for retrieval and iii) the retrieval time is determined by the time to reach threshold of one or a group of neurons. iv) The time to produce the first spike after input starts is determining the response time.

We investigate here if this model hypothesis is consistent with the participants' decrease in retrieval time with increased D, and with the variability of the response times.

[3] With 11 subjects, producing 12 responses for each delay in each of 3 sessions, we have 396 measurements for each delay.

5.1 Speed of synaptic learning.

5.1.1 Physiological data.

There is little experimental information on the speed of synaptic changes in biology. In this section we estimate the learning speed from synaptic depression and spine growth data, to determine how fast weight changes can actually take place at the single synapse level. A theoretical model of learning is presented in section 5.1.2.

Learning speed estimation from synaptic depression. Given that Long Term Potentiation (LTP) requires the insertion of new AMPA receptors in the synapse, information on the speed of the process can be gained from observing the recovery from synaptic depression, although it is difficult to separate pre-synaptic vesicle replenishing effects, postsynaptic AMPAR recovery processes and diffusive contributions. Recovery is probably dominant for large synapses while diffusion and vesicle depletion dominate for small synapses (Heine et al., 2008). When intracellular calcium concentration is increased through NMDA activation, the recovery from depression is slowed down, indicating that diffusion effects can be the limiting factor in the recovery time from depression. Thus, recovery time constants from depression represent a lower bound on the receptors influx time during learning. From data published in (Heine et al., 2008), the full synaptic conductivity is restored in approximately 200ms.

Estimation from the speed of growth of new spines. There is a good correlation between synapse area and number of AMPA receptors in a synapse (Takumi et al., 1999). Therefore, another source of information on the speed of learning is the observation of the speed of growth of spines. Several experiments have shown very fast growth of new spines in the presence of glutamate produced by uncaging. In Kwon and Sabatini (2011), a spine can grow to a length of 1um with an average spine head area of 0.4um2 in as little as 10 seconds. This is produced by 20 uncaging pulses produced at 2Hz. The same growth can be produced by 20 pulses at 0.5Hz, in a total time of 40 sec. The process requires NMDA activation. The independence of pulse frequency suggests that a certain amount of growth occurs for each pulse with a rate of membrane area addition of at least 0.23um2/sec. In Takumi et al. (1999) synapses with a radius of 0.1um have no AMPAR, and are deemed “silent”, while those with 0.2um have a maximum number and are fully functional. The area difference between these two states is 0.19um2, which could be grown in just less than 1 second.

Implications for fast learning. The data presented above provide a maximum time of learning per synapse of 1 sec based on spine growth and a minimum of around 200ms defined by the recovery time from depression. With an input stimulus firing at around 50Hz, these boundaries allow for between 10 and 50 spikes to induce the desired synaptic weight. These speeds are estimated for learning using existing synapses starting from a silent state. Growing new spines would take at least around 10secs. Very fast synaptic weigh changes, in around 200ms, appear to be achievable by the diffusion of receptors into the synaptic cleft.

5.1.2 *Modelling the time course of synaptic learning.*

We assume that each input spike caused the addition of receptors to a synapse. These receptors are taken from a limited pool W_P of receptors available at the surface of the neuron's membrane. Each spike collects a fraction ω of the pool and reduces the size of the pool by the amount collected. The rate of pool reduction by *n* input spike trains firing with a frequency F_{IN} is given by:

$$\frac{dW_P}{dt} = -W_P \cdot \omega \cdot n \cdot F_{IN} \qquad (10)$$

As a consequence, the pool decays exponentially with time as:

$$W_P(t) = W_P(0) \cdot \exp(-t \cdot \omega \cdot n \cdot F_{IN}) \qquad (11)$$

The weight resources not contained in the pool are naturally distributed between all active synapses[4], and learning is deemed completed when the pool is empty. The learning time constant t_L is given by

$$t_L = \frac{1}{\omega \cdot n \cdot F_{IN}} \qquad (12)$$

After a duration $5*t_L$, 99.3% of the pool resources has been transferred to synapses. The estimation above tells us that his takes at least 200ms, i.e. $t_L > 40$ms.

Assuming a total available weight resource W_0, each learning synapse will have its weight W_L increasing as:

$$W_L(t) = W_L(0) + \frac{1}{n}(W_0 - W_P(t)) \qquad (13)$$

For simplicity we will assume that all the n weights have the same value. The sum of their starting values $W_L(0)$ is the difference between the starting pool size $W_P(0)$ and the full pool W_0:

$$W_P(0) = W_0 - n \cdot W_L(0) \qquad (14)$$

Thus

$$W_L(t) = W_L(0) + \frac{1}{n}(W_0 - (W_0 - n \cdot W_L(0)) \cdot \exp(-t / t_L) \qquad (15)$$

Rewriting the initial learning weight $W_L(0)$ as a fraction β of W_0/n we obtain:

$$W_L(t) = \frac{W_0}{n}[1 - (1 - \beta)\exp(-t / t_L)] \qquad (16)$$

[4] The weight increase is faster for more active inputs, leading to larger weights for these inputs. For simplicity we will assume here that all input fire at the same rate and all weight will therefore be roughly equal.

5.2 Neuronal firing time and variability

5.2.1 Neuron model

The leaky integrate-and-fire (LIF) neuron model is summarized in figure 9. A full description of the equations describing its operation is given in Bugmann (2012) . Here we used the LIF model with balanced synaptic depression (τ_{rec} = RC_{SOMA} = 50ms). This balancing ensures a maximal variability of the first spike, by removing most of the temporal integration effects, making the neuron a coincidence detector. The neuron was simulated with 8 inputs, a number that generates the same behaviour as a larger number of inputs and enables short simulation times. The threshold is set to 15mV. The simulation time step was 1 ms.

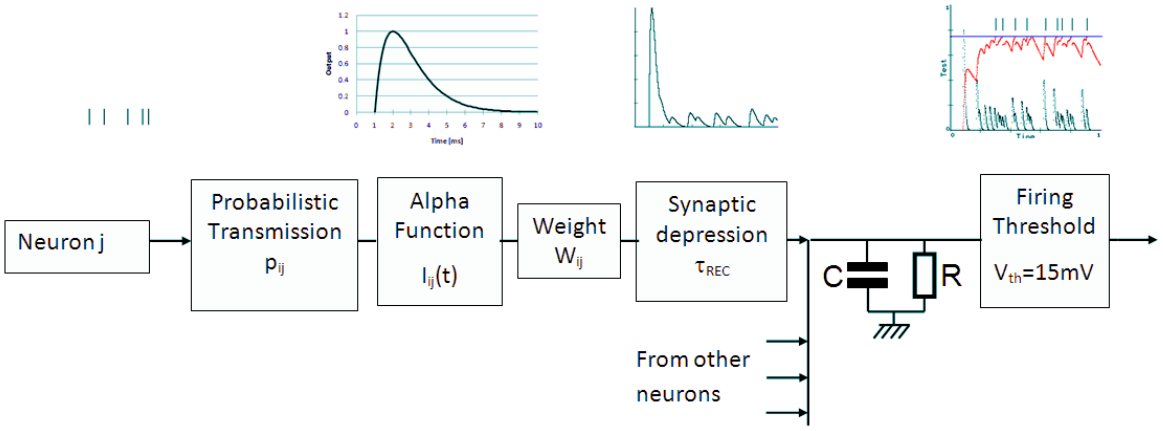

Figure 9. Diagrammatic description of the leaky integrate-and-fire neuron model used. Inputs from neuron j are Poisson spike trains with a frequency of 30Hz. The synapse has a transmission probability p_{ij}=0.9. The synaptic current is modelled as an alpha function with a maximum at 1 ms after arrival of the input. An axonal transmission delay of 1 ms is implemented. The synapse exhibits synaptic depression with a recovery time constant of τ_{rec} = 50ms. The soma is modelled as a RC circuit with time constant RC_{SOMA}=50ms.

5.2.2 Simulations

We ran simulations of the balanced LIF model to examine if the experimental relation between the average response time and its standard deviation could be explained by a LIF model with synaptic learning.

The variability of the firing time has at least two causes: The variability of the total synaptic weight achieved after a fixed learning time and the variability of the firing time due to the random passage of the firing threshold. Both processes were included in our simulations.

First, we let the synaptic weights increase with 8 inputs firing at 30Hz (this frequency is appropriate for the areas considered (TE to Hippocampus). We did not let the neuron fire in this phase. The maximum possible weight was set to W_0=12. The time of learning was limited to values between 70 and 120ms, to achieve a range of response times similar to those in figure 8B. It should be noted

that the values of the learning times are not significant here. Different learning times could have been used with a different rate of weight increase. Here we used ω= 0.08 (see equation 10).

In a second phase, we reset the neuron (V_{SOMA} = 0 and synapses fully recovered). Then, using the grown synaptic weights, we activated the same 8 inputs, and let the somatic potential grown until the first spike was produced.

These two phases constituted a run. 100 runs were conducted for each set learning time. These 100 times to fire the first spike allowed to calculate a set of average firing time values and their standard deviations, as shown by curve labelled "1 output" in figure 10. It should be noted that an increase in the number of simulations from 25 to 50 and 100 did not generate more aligned points. This was traced back to the very skewed distribution of firing times generated by the simulations, with some very long firing times occurring. To generate points with a better alignment for figure 10, we applied the same filtering rule used for eliminating "outliers" in experimental data, namely removing data points larger than 2.5 standard deviations above the initial average value. While long delays generated by simulation are definitely not "outliers", it makes sense to apply the same data pre-processing to two sets of data that are to be compared.

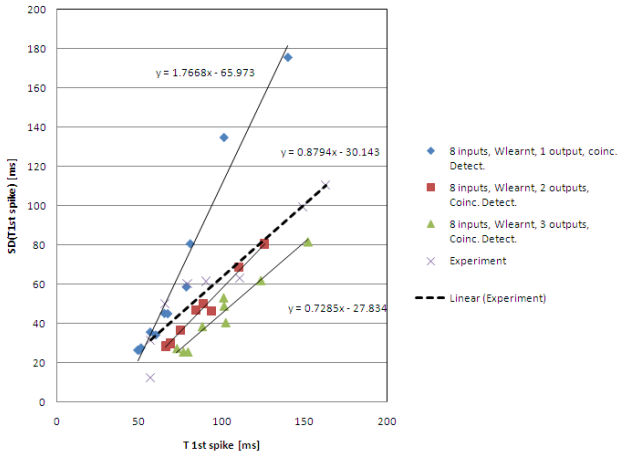

A)

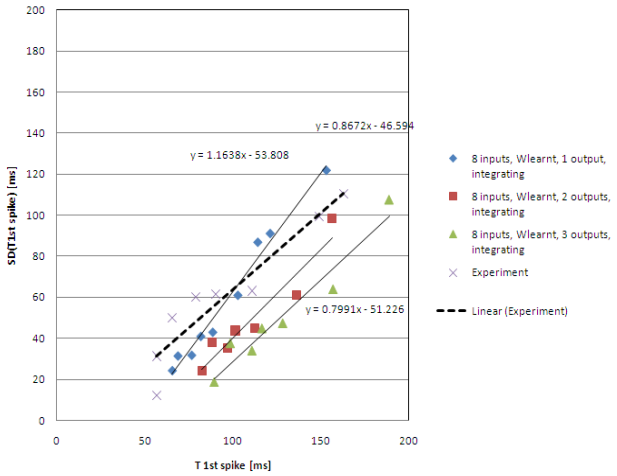

B)

Figure 10. Result of simulating learning and firing with a LIF neuron model. The dotted line reproduces the experimental result in figure 8B. **A**. Using a balanced LIF model, τ_{rec}=50ms, *RC*=50ms, behaving as a coincidence detector. **B**. Using an integrating LIF neuron, τ_{rec}=20ms, *RC*=75ms,

These initial simulations show a slope of *SD(T)* much larger than the experimental one. I may be noted that this is due to the variability of the weights generated during learning simulations. When the same simulations were done with a range of set initial weights, instead of a range of learning times, the *SD(T)* slope was much lower, comparable to the one in figure 8B. Another way to reduce the slope is to assume that the response is caused by *m* first spikes produced by *m* independent neurons. To determine the slope that would be generated by a pool of m=2 and m=3 output neurons, we divided results of the simulations into 50 sets of 2 firing times and 33 sets of 3 firing times. The longest of the *m* times was considered to be the time of response initiation. The resulting average times and their SD are shown in figure 10.

Figure 10A can be interpreted with the help of the results in figure 8A. The experimental curve is to the left of those of the simulated underlying processes with 2 and 3 outputs. This is consistent with a model where simple RT and retrieval processes are both using the hippocampus route. The simulation curve for the one-output model has a slope too different from the experimental one to be considered. A smaller slope can be achieved with a LIF model with more temporal integration (figure10B). The main effect of increased temporal integration is to move the curves of the simulated underlying process to the right of the experimental curve, strengthening the case for the hippocampus route.

The lateral shift predicted by the theory (section 4) is equal to the minimum response time of a fully trained neuronal system with m outputs. This consists of the shortest response time of a fully trained neuron, typically 10ms (Thorpe et al., 1996) and an additional 16ms delay for m=2 or 25ms for m=3 (average values of data plotted in figure 10). Thus the lateral shift should be of around 26 ms for m=2 and 35ms for m=3. The shift values in figure 10 are 20ms for the coincidence detection neuron and 33ms for the integrating neuron. Thus, both neuron operations modes are consistent with the experimental data, assuming a pool of 2 or 3 independent rule encoders. As noted in (Britten et al., 1992), if output neurons were not truly independent, a much larger number of them would be needed to achieve the same result.
The similarity between the slopes of experimental and simulated data, and a time shift between simulation and experiment consistent with theoretical expectations give a broad support to the neural model hypotheses, namely learning through randomly timed synaptic weights increments and response through random reaching of the firing threshold.

5.3 Time course of learning.

The simulations provide data to relate the time of firing the first spike with the total synaptic weight. This relation can then be used to estimate the values of experimental synaptic weights for various delays D. Figure 11 shows how total synaptic weights influence the time to producing the first spike. The integrating model operates with lower weights, as the inputs are integrated over time. The coincidence detecting neuron needs larger weights, as short term events trigger firing. To analyse experimental data we focused on the functions fitting curves for m=3. For the integrating neuron:

$$T_{1st} = 256 \cdot (W - 3.7)^{-0.96}, \qquad (17)$$

and for the coincidence detecting neuron:

$$T_{1st} = 335 \cdot (W - 6.5)^{-1.12} \qquad (18)$$

The values 3.7 and 6.5 are the minimum total weights that are need to elicit output spikes of these two neuron models, albeit with very long latencies.

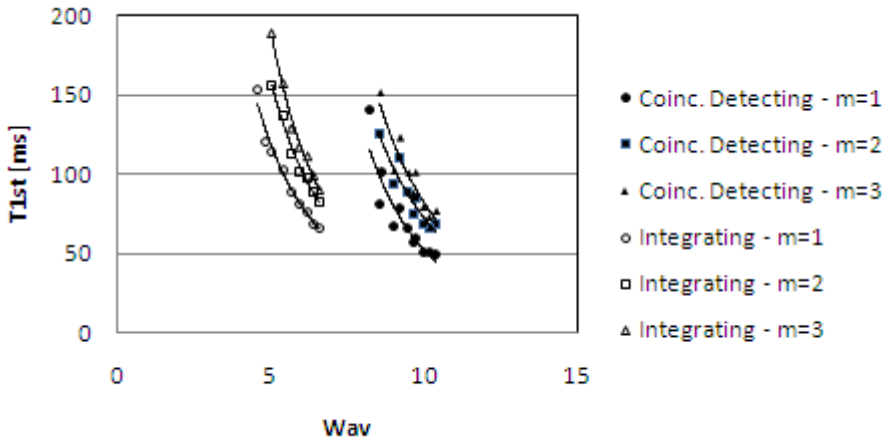

Figure 11. Relation between firing time and total synaptic weights for the coincidence detecting (balanced) LIF model and the integrating LIF model. The three sets of data for each model correspond to pools of m-1, 2 and 3 output neurons.

We inverted formulas (17) and (18) to calculate the weights corresponding to the average response times over sessions 2, 3 and 4 shown in figure 3, that depicts the response times from which the simple reaction time has been subtracted. We added the estimate value of T_{20}=10ms to these values to comply with the anatomical all-hippocampus model (equation (7) in section 4).

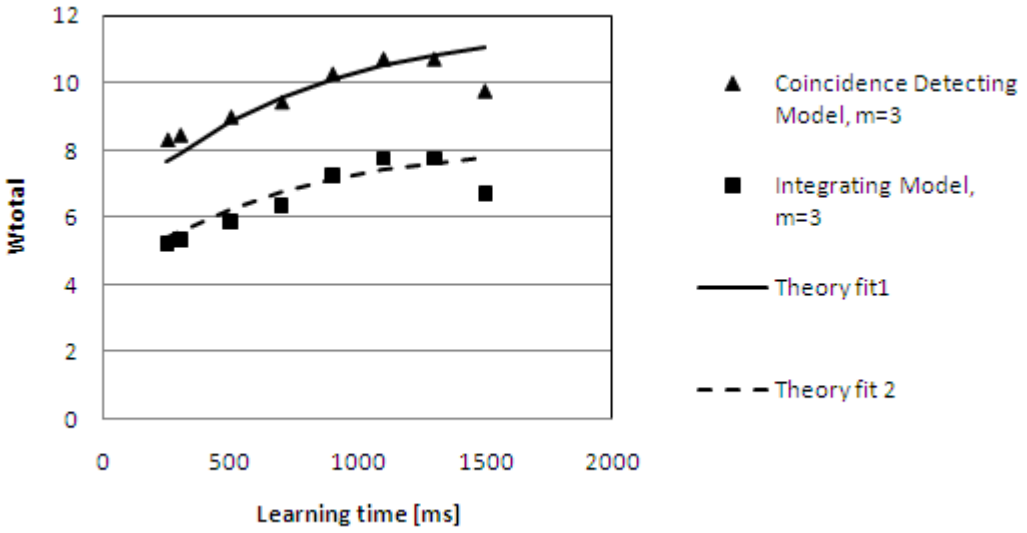

Figure 12. Weights for LIF neurons in a pool of 3 that explain the behavioural response times in figure 3 (average times over sessions 2, 3 and 4). Two sets of values have been calculated by assuming either coincidence detecting neurons or integrating neurons. The lines are fits to the data with the theory of synaptic learning in section 5 (equation 16).

The two curves in figure 12 are produced by our model of synaptic learning (equation (16) in section 5.1.2) with parameters given in table 1. The fits are reasonably good, except for the point at 1500ms where subjects showed signs of loss of memory of the encoded rule. It is noteworthy that the learning rate during the delay is insufficient to account for a full increase during the SR rule presentation period. This is reflected in the β parameter indicating that synapse have an initial weight of half the maximum total weight at time 0. This may be the case, but is unlikely, at least for the integrating model, as the initial weight is above the minimal weight necessary for the neuron to become responsive. Another possibility is that learning is much faster during SR rule presentation. During that time, rule encoding neurons receive actual sensory input, and are able to fire at a high rate. During the delay, we assumed that these neurons were activated by memory firing in PFC that may support a much weaker activity in these neurons. Therefore, the curves in figure 12 appear to be consistent with our hypotheses. Indeed, future measurements with shorter SR rule presentation times would allow testing the model further.

The results show that our model can explain the data with two sets of model parameters in quite different regimes of operation of the LIF neuron model. This indicates the robustness of our approach.

Table 1. Parameters of the synaptic learning model fitting the calculated experimental weight increase with learning time.

	Fit to weights generated by the coincident detection model	Fit to weights generated by the temporal integration model
Maximum total weight resources available. W_0	11.8	8.3
Initial fraction of total resources already allocated to synapses: β	0.5	0.5
Learning rate: $n * \omega * F_{IN}$	1.4	1.4

6 Discussion

In this experiment, participants had to process two sets of instructions. 1. At the start of the experiment, they were instructed to interpret an image as an instruction, then to interpret a second image as a response request. 2. During the experiment, they processed a series of visual instructions presented. The first instruction process puts in place a control network with connections and switches that manage the behaviour during the experiment, including processing the visual instructions. This paper focuses on the dynamics of how participants process the visual instructions. This is a much simpler problem than understanding how the first instruction set is implemented, that engages a much larger network of brain areas, from language areas to multiple prefrontal areas (see e.g. Dumontheil et al., 2011).

This paper reports on what is probably the first experiment designed to measure the speed of learning from instructions. The results are surprising because they show that learning the stimulus-response association appears to have been completed to a large extent within 250 ms (fig. 12). This value is a very short time close to the physiological limit for monosynaptic learning estimated from

the dynamics of recovery from synaptic depression. The results show the anticipated prolonged response times for very short delays.

There is a clear reduction of response times between session 1 and sessions 2,3 and 4. (fig. 3). It is not clear what mechanism is causing this. A reduction in response time with practice has been observed by Ruge and Wolfensteller (2010) when applying the same SR rules repeatedly. A similar reduction has also been related to faster response learning in the literature on priming (Dobbins et al., 2004).

To explain the shape of the response time curves, we developed a model of learning and response generation. This model has several innovative features. First it was assumed that associative learning is not directly linking the stimulus to the motor response, but linking the visual representations of the stimulus and of response. The associative activation of the response representation then in turn activates the motor response. This restricts the learning requirements to local connections within a cortical area. The fact that the model suggests incomplete learning and the short learning time by subjects restricts the learnt connections to be monosynaptic, as opposed, e.g., to connections in a multilayer model of successive brain areas (Bugmann, 2012).

The second innovative element of the model is to combine the randomness of synaptic weights generated in a Hebbian way with the randomness of the crossing time of the firing threshold to explain the variability of the behavioural response times. This is the simplest possible model, given our knowledge of neurophysiology. Its predictions regarding the number of neurons needed to encode the rule is consistent with other works showing that perceptual judgements are based on “a small number of independent neural signals” (Britten et al, 1992) or “no more than a few cells” (Zohary and Hillman, 1990).

The results on the time course of synaptic modification suggest that fast learning may be taking place during the presentation of the SR rule, followed by slower learning during the delay period. The later may be supported by persistent activity in PFC that feeds back to IT (Rempel-Clower and Barbas , 2000). To test this hypothesis calls for measurements with shorter SR presentation times. Issues of prolonged firing of sensory neurons may complicate such measurement.

A problem not considered here, and in most models, is unlearning. The new weights should really disappear before a new SR rule is presented. Several participants reported a difficulty in remembering the SR rule for long delays (1100 ms and 1300 ms). It is possible that the learnt weights decay within a few seconds. Future experiments with longer delays could shed light on the duration of SR encoding.

The problem of generating responses from partially trained weights is not too dissimilar from the problem of responding to incomplete sensory stimuli. An examination of the literature in this area (e.g. Wilson, 2009) could shed some light on the most likely mechanism to be at work in fast learning and responding. Results by Bugmann (2007) show that visual neurons need less than 50% of their inputs to be active to start firing. This low selectivity enables them to respond rapidly when all inputs are present and still respond, but with longer delays, to incomplete patterns.

Other models deal with the problem of mapping sensory input to motor outputs. In the models by (Hamker, 2005; Huang et al., 2013; Deco and Rolls, 2005) a similar network of brain areas as ours is

used. In the works of Zylberberg et al., (2010) a more abstract architecture is analysed. Hamker (2005) addresses the delayed matching-to-sample problem without using synaptic learning. Sustained top-down firing is used to bias the competition between subsequently presented patterns. This is not a suitable mechanism to encode S-R associations. Huang et al. (2013) propose a dual-route model. Fast learning and slow processing is using a route from hippocampus to basal ganglia, PFC and PM. Slow learning but fast processing is using the PPC and its link to PM. However, learning in both routes is too slow for our data. The hippocampal route requires around 5 repetitions of an instruction to store it correctly and the PPC route requires replays of stimulus-to-action rules by the hippocampus to slowly build "habits". In the model by Deco and Rolls (2005) S-R rules are represented by existing pools of neurons in the PFC, and rules are selected through a biased competition. The creation of pools, i.e. the encoding of instructions, is not modelled. Zylberberg et al. (2010) also assume a pre-existing representation pool for all possible S-R combinations. Other models using reinforcement learning are too slow for our purpose. The approach by Huang et al., (2013) appears the most promising for modelling our data, but its hippocampus learning model is quite complex and would need re-examining in view of the fast one shot learning shown here.

7 Conclusion

The new experiment described here clearly shows an increase in response times when instructed stimulus-response associations are tested within 300ms to 700ms after the start of the instruction. All participants were able to respond with a low error rate after only 250ms of available learning time. It is proposed here that the diffusion of AMPA receptor into the synaptic cleft is a mechanism fast enough to explain the data.

A robust neural model has been proposed that explains the increase of response time and their variability using simple mechanisms of synaptic learning assuming a limited total available weight resource, followed by random crossing of the firing threshold produced by random inputs. A pool of 2 or 3 of such independent neurons can explain the behavioural responses. Such small numbers have been reported elsewhere for perceptual discrimination tasks. Indeed, much larger number may be needed to produce the same results if they are not truly independent, e.g. due to shared inputs.

In summary, this work presents the first measurement of the speed of learning SR associations and proposes a compact and testable model to explain the observations.

Acknowledgments: The authors are grateful for the reviewers comments and for the enlightening discussions with Rana Moyeed about random processes.

References.

Borra E, Belmalih A, Calzavara R, Gerbella M, Murata A, Rozzi S, Luppino G. 2008. Cortical connections of the macaque anterior intraparietal (AIP) area. Cereb Cortex 18:1094–1111.

Borra E, Gerbella M, Rozzi S, Luppino G. 2011. Anatomical evidence for the involvement of the macaque ventrolateral prefrontal area 12r in controlling goal-directed actions. J Neurosci 31:12351–12363.

Britten KH, Shadlen MN, Newsome WT and Movshon A. 1992. The analysis of visual motion: A comparison of neuronal and psychophysical performance. The journal of neuroscience. 12(1): 4745-4765.

Brasted PJ, Bussey TJ, Murray EA, Wise SP (2003) Role of the hippocampal system in associative learning beyond the spatial domain. Brain 126:1202–1223.

Bugmann G. 2007. Fraction of excitatory inputs required by a visual neuron to fire. Biosystems 89:1-3, p.154-159.

Bugmann G. 2009. A Neural Architecture for Fast Learning of Stimulus-Response Associations. Proceeding of IICAI'09, Tumkur (Bangalore), pp 828-841.

Bugmann G. 2012. Modelling fast stimulus-response association learning along the occipito-parieto-frontal pathway following rule instructions. Brain Research, vol.1434, pp. 73-89.

Bunge SA, Hazeltine E, Scanlon MD, Rosen AC, Gabrieli JD. 2002. Dissociable contributions of prefrontal and parietal cortices to response selection. Neuroimage 17:1562--1571.

Bussey, T. J., Wise, S. P., & Murray, E. A. 2002. Interaction of ventral and orbital prefrontal cortex with inferotemporal cortex in conditional visuomotor learning. Behavioral Neuroscience, 116, 703–715

Cole M.W., Bagic A., Kass R., Schneider W. 2010. Prefrontal Dynamics Underlying Rapid Instructed Task Learning Reverse With Practice. Journal of Neuroscience 30(42):14245-14254.

Deco G. and Rolls ER. 2005. Attention, short-term memory, and action selection: a unifying theory. Prog Neurobiol, 76(4):236-56

Dobbins IG , Schnyer DM , Verfaellie M , Schacter DL. 2004. Cortical activity reductions during repetition priming can result from rapid response learning. Nature 428:316–319.

Dumontheil I, Thompson R, Duncan J. 2011. Assembly and use of new task rules in fronto-parietal cortex. J Cogn Neurosci 23(1):168-82.

Furtak, S. C., Wei, S. M., Agster, K. L., & Burwell, R. D. 2007. Functional neuroanatomy of the parahippocampal region in the rat: the perirhinal and postrhinal cortices. Hippocampus, 17(9), 709-722.

Fuster JM, Bauer RH, Jervey JP (1985) Functional interactions between inferotemporal and prefrontal cortex in a cognitive task. Brain Res 330:299–307.

Gelbard-Sagiv H, Mukamel R, Harel M, Malach R, Fried I. 2008. Internally generated reactivation of single neurons in human hippocampus during free recall. Science 322:96–101.

Grafton ST. 2010. The cognitive neuroscience of prehension: Recent developments. Experimental Brain Research, 204 (2010), pp. 475–491

Hamker, F. H. 2005. The Reentry Hypothesis: The Putative Interaction of the Frontal Eye Field, Ventrolateral Prefrontal Cortex, and Areas V4, IT for Attention and Eye Movement. Cerebral Cortex, 15: 431-447.

Hartstra E. , Waszak F, and Brass M. 2012. The implementation of verbal instructions: Dissociating motor preparation from theformation of stimulus–response associations. NeuroImage 63: 1143–1153.

Heine M, Groc L, Frischknecht R, Beique JC, Lounis B, Rumbaugh G, Huganir RL, Cognet L, Choquet D. 2008. Surface mobility of postsynaptic AMPARs tunes synaptic transmission. Science 320, 201-205.

Hopfield J.J. 1982. Neural networks and physical systems with emergent collective computational abilities. *Proceedings of the National Academy of Sciences of the USA*, vol. 79 no. 8 pp. 2554–2558.

Huang T-S, Hazy TE., Herd SA., and O'Reilly RC. 2013. Assembling Old Tricks for New Tasks: A Neural Model of Instructional Learning and Control. Journal of Cognitive Neuroscience. Posted Online February 5, 2013. (doi:10.1162/jocn_a_00365)

Kealy, J. and Commins, S. (2011) The rat perirhinal cortex: A review of anatomy, physiology, plasticity, and function. Progress in Neurobiology, 93:522-548.

Kwon HB, Sabatini BL. 2011. Glutamate induces de novo growth of functional spines in developing cortex. Nature 474: 100-104.

Mathôt S., Schreij D., and Theeuwes J. 2012. OpenSesame: An open-source, graphical experiment builder for the social sciences. Behav Res. 44:314–324.

Messinger A, Squire LR, Zola SM, Albright TD. 2005. Neural correlates of knowledge: stable representation of stimulus associations across variations in behavioral performance. Neuron 48:359-71.

Mruczek REB & Sheinberg DL. 2007. Activity of inferior temporal cortical neurons predicts recognition choice behavior and recognition time during visual search. J Neurosci, 27, 2825-2836.

Naber PA, Witter MP, Lopes da Silva FH. 1999. Perirhinal cortex input to the hippocampus in the rat: evidence for parallel pathways, both direct and indirect. A combined physiological and anatomical study. Eur J Neurosci 11:4119–4133.

Naya, Y., Sakai, K. and Miyashita, Y. 1996. Activity of primate inferotemporal neurons related to a sought target in pair-association task. Proc. Natl. Acad. Sci. USA, 93, 2664-2669.

Osada T, Adachi Y, Kimura HM, Miyashita Y. 2008. Towards understanding of the cortical network underlying associative memory. Philos Trans R Soc Lond B Biol Sci. 363(1500): 2187–99.

Passingham RE, Toni I, Rushworth MF. 2000. Specialisation within the prefrontal cortex: the ventral prefrontal cortex and associative learning. Exp Brain Res. 133(1):103-13.

Passingham R.E. and Toni I. 2001. Contrasting dorsal and ventral visual systems: guidance of movement versus decision making. NeuroImage 14, S125-S131

Ranganath C, Cohen MX, Dam C, D'Esposito M. 2004. Inferior temporal, prefrontal, and hippocampal contributions to visual working memory maintenance and associative memory retrieval. J. Neurosci. 24, 3917–3925

Rempel-Clower N.L. and Barbas H. 2000. The Laminar Pattern of Connections between Prefrontal and Anterior Temporal Cortices in the Rhesus Monkey is Related to Cortical Structure and Function . Cereb. Cortex, 10 (9): 851-865.

Rolls ET and Xiang J-Z. 2006. Spatial view cells in the primate hippocampus, and memory recall. Reviews in the Neurosciences. 17:175–200.

Ruge, H., and Wolfensteller, U. 2010. Rapid formation of pragmatic rule representations in the human brain during instruction-based learning. Cereb Cortex, 20, 1656–1667.

Sakata H., Taira M., Kusunoki M., Murata A., and Tanaka Y. 1997. The TINS lecture: the parietal association cortex in depth perception and visual control of hand action. Trends in Neurosciences, vol. 20, no. 8, pp. 350–357.

Takumi Y, Ramirez-Leon V, Laake P, Rinvik E, Ottersen O.P. 1999. Different modes of expression of AMPA and NMDA receptors in hippocampal synapses. Nat Neurosci 2:618–624.

Thorpe S, Fize D, Marlot C. 1996. Speed of processing in the human visual system. Nature 381 (6582), 520-522.

Ungerleider, L.G., Galkin, T.W., Desimone, R., and Gattass, R. 2008. Cortical connections of area V4 in the macaque. Cerebral Cortex 18: 477-499.

Wilson DA. 2009. Pattern completion in olfaction. International symposium on olfaction and taste. Ann. N.Y. Acad. Sci. 1170:306-312.

Wolfensteller, U. and Ruge, H. 2012. Frontostriatal mechanisms in instruction-based learning as a hallmark of flexible goal-directed behavior. *Front. Psychology* 3:192.

Yamagata T, Nakayama Y, Tanji J, Hoshi E. 2012. Distinct information representation and processing for goal-directed behavior in the dorsolateral and ventrolateral prefrontal cortex and the dorsal premotor cortex, J Neurosci., 32(37)：12934-49.

Zironi I, Icovelli P, Aicardi G, Liu P, Bilkey DK. 2001. Prefrontal cortex lesions augment the location-related firing properties of area TE/Perirhinal cortex neurons in a working memory task. Cereb Cortex, 11, pp. 1093–1100

Zohary E, Hillman P and Hoschstein S. 1990. Time course of perceptual discrimination and single neuron reliability. Biol. Cybernetics. 62, 475-486.

Zylberberg A, Fernandez Slezak D, Roelfsema PR, Dehaene S, Sigman M (2010) The Brain's Router: A Cortical Network Model of Serial Processing in the Primate Brain. PLoS Comput Biol 6(4): e1000765. doi:10.1371/journal.pcbi.1000765